RSC Advances

ROYAL SOCIETY OF CHEMISTRY

www.rsc.org/advances

RSC Advances

ARTICLE

Table of contents

Grafting Ni particles onto SBA-15, and their enhanced performance for CO_2 methanation

Baowang Lu, Yiwen Ju, Takayuki Abe and Kastuya Kawamoto

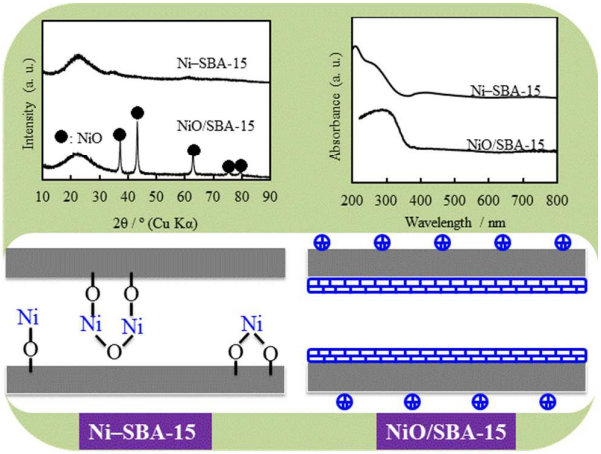

Ni particles could be grafted onto SBA-15 through a bond –O–Ni–O–Si–O– formation using $(Ni(NH_3)_x)^{2+}$.

RSC Advances

ARTICLE

Grafting Ni particles onto SBA-15, and their enhanced performance for CO_2 methanation

Received 00th January 20xx,
Accepted 00th January 20xx

DOI: 10.1039/x0xx00000x

www.rsc.org/

*Baowang Lu,[*a] Yiwen Ju,[b] Takayuki Abe[a] and Katsuya Kawamoto[c]*

By a post synthesis method, nickel (Ni) particles could be grafted onto SBA-15 for the first time through a chemical bond (–O–Ni–O–Si–O–) formation between silicon (Si) and Ni via oxygen (O) using Ni ammonia (NH_3) complex ions $(Ni(NH_3)_x)^{2+}$ with NH_3/Ni mole ratio of 1~5, which existed as Ni phyllosilicate on SBA-15 surface, while Ni particles could not be grafted onto SBA-15 in the absence of NH_4OH (NH_3/Ni mole ratio of 0). NH_3/Ni mole ratio of 2~4 was suitable grafting conditions, which could give a product with the closest Ni amount to raw. This product obtained was named Ni-grafted SBA-15 sample. XPS, UV-vis and H_2-TPR analyses demonstrated that a chemical bond was formed between Ni and silicon (Si) via oxygen (O), and no bulk nickel oxides existed in Ni-grafted SBA-15 sample. The formation of –O–Ni–O–Si–O– was completed via the reaction between hydrolyzate $Ni(OH)(NH_3)_{x-1})^+$ from $(Ni(NH_3)_x)^{2+}$ and ≡Si–OH (silanol sites) on SBA-15 surface. Ni-grafted SBA-15 catalyst suited CO_2 methanation, resulting in higher CO_2 conversion and methane selectivity than NiO dispersed SBA-15 catalyst obtained by conventional post synthesis method. The activation energy for CO_2 methanation increased with decreasing initial Ni amount used. The rate equation for CO_2 methanation could be expressed as: $r = kC_{CO_2}^{0.64}C_{H_2}^{4.05}$, C was concentration. Ni-grafted SBA-15 catalyst had high thermal stability for CO_2 methanation.

1 Introduction

The discovery of mesoporous molecular sieves (MMS) as catalysts or catalyst supports has opened a new research area. Ordered MMS are not often used as catalysts. Much more frequently, transition metal is introduced to add its catalytic functions.[1,2] Transition metal can be introduced into MMS either from the starting synthesis mixture during MMS synthesis process using a direct synthesis method[3-7] or by post synthesis modification.[8-18] By post synthesis method, transition metal nanoparticles as oxides generated on MMS typically lack uniformity as regards size and shape due to particle aggregates, which often exhibit low catalytic efficiency because not every active center can play its catalytic role and thus a large number of active centers is wasted. By direct synthesis method, transition metal nanoparticles incorporated into MMS catalysts exhibit greatly enhanced catalytic activity owing to the maximum dispersion of their active centers and a strong metal-support interaction.[3,19-21] Thus and so, to ensure each transition metal nanoparticles can play its full catalytic role, to achieve their maximum dispersion (incorporating them into MMS) is very important for improving catalytic efficiency, and the direct hydrothermal synthesis method is only way at current. Therefore, the incorporation of transition metal into MMS structure is extremely expected, and a lot of effort has been focused on this topic using a direct synthesis method[3-6,22-25] or by a template ion exchange approach.[26]

The mechanism for realizing transition metal incorporated MMS is the formation of a chemical bond (–O–M–O–Si–O–) between silicon (Si) and metal (M) via oxygen (O). Because SBA-15 is commonly synthesized in strong acid media,[27] it is difficult to obtain transition metal nanoparticles incorporated into SBA-15 by direct synthesis method due to almost no formation of –O–M–O–Si–O– in acid media, and highly dispersed oxides is often obtained.[7,28] However, there is still no report on grafting transition metal onto SBA-15 surface through the formation of –O–M–O–Si–O– using a post synthesis method.

As one transition metal, nickel (Ni) shows good catalytic activity, and various supports (SiO_2, Al_2O_3, TiO_2) can markedly improve its catalytic activity due to well-dispersed active centers generated on porous hosts.[29] Therefore, Ni-based catalysts remain the most extensively studied materials. Recently, highly dispersed NiO/SBA-15 can be prepared by either direct synthesis method[7,28] or post synthesis method.[18,22,23] However, each Ni cannot play its role duo to aggregate, exhibits low catalytic efficiency. Therefore, to enhance Ni catalytic efficiency, developing a fresh approach for grafting Ni onto SBA-15 surface remains an important and interesting topic.

Che et al. has investigated Ni ion strongly interact with silica support applying an ion exchange approach, and silicate formation have been suggested.[30] To prevent the precipitation of $Ni(OH)_2$ or the decomposition of Ni complexes, the wash with solutions containing 1M NH_4NO_3 and at the pH of the supernatant solutions was needed after exchange. In the case of ordered mesoporous silica support, the crucial difference with silica support is not only preventing the precipitation of $Ni(OH)_2$ or the decomposition of Ni complexes, but also maintaining the ordered structure to obtain high catalytic performance. Therefore, it is more difficult to obtain Ni ion strongly interact with ordered mesoporous silica support, and there is still no study on Ni ion strongly interacts with ordered mesoporous silica support using a simple method.

[a] *Hydrogen Isotope Research Center, Organization for Promotion of research, University of Toyama, 3190 Gofuku, Toyama, 930-8555, Japan. E-mail: baowangl@ctg.u-toyama.ac.jp; Tel: +81-76-445-6933*
[b] *Laboratory of Computational Geodynamics College of Earth Science, University of Chinese Academy of Sciences, Beijing 100049, China.*
[c] *Graduate School of Environmental and Life Science, Okayama University, 3-1-1 Tsushima-naka, Kita-ku, Okayama-shi, Okayama, 700-8530, Japan.*

Here, we investigated how to graft Ni onto SBA-15 surface through the formation of –O–M–O–Si–O– using a post synthesis method. Various analysis tecniques, such UV-vis XPS, H_2-TPR and FT-IR were employed to study the formation of –O–M–O–Si–O–. The carbon dioxide (CO_2) methanation was also carried out further to evaluate the catalytic performance of Ni grafted SBA-15 catalyst.

2 Experimental section

Synthesis of catalysts

SBA-15 was first synthesized by a modifying method.[31] 16 g of Pluronic P123 (P123, $EO_{20}PO_{70}EO_20$, Aldrich, USA) was dissolved in 410 g of deionized water at room temperature in a Teflon autoclave, then 42.08 g of tetraethylorthosilicate ($Si(OC_2H_5)_4$, TEOS, Junsei Chemical, Japan, 95.0 %) was added. After stirring for 30 min, 114.4 g of hydrochloric acid (HCl, Junsei Chemical, Japan, 35.0~37.0 %) was added to obtain the starting synthesis mixture. The starting mixture was aged immediately at 80 °C for 24 h under stirring condition. The product was filtered, washed, dried overnight in an oven at 80 °C, and then calcined at 550 °C for 10 h.

In 30 g of deionized water, nickel (Ni) ammonia (NH_3) complex ions with different NH_3/Ni mole ratios were prepared using nickel (II) nitrate hexahydrate ($Ni(NO_3)_2{\bullet}6H_2O$, 98%, Wako, Japan) and NH_3 solution (28~30.0%, Kishida, Japan). 3 g of SBA-15 was added into the above complex ion solution and stirred ≈ 30 min, then grafted 48 h under a static conditions. The solid product grafted was filtered, washed thoroughly with deionized water, dried overnight at room temperature, and calcined at 500 °C for 5 h.

Characterization

The X-ray diffraction (XRD) patterns of the products were collected by a powder X-ray diffractometer (Rigaku Multiflex) with graphite monochromatized Cu Kα radiation at 40 kV and 26 mA. Nitrogen (N_2) adsorption isotherms at -196 °C were obtained using a conventional volumetric apparatus (Quadrasorb USA). Before the adsorption measurements were made, the powders (≈ 0.1 g) were subjected to a temperature of 300 °C for 5 h in a vacuum. The specific surface area was calculated with the Brunauer-Emmett-Teller (BET) method. The pore size was calculated from the desorption branch of nitrogen adsorption-desorption isotherms by the Barrett-Joyner-Halenda (BJH) method. The pore volume was taken at a single point P/P_0 = 0.95. The solid product was observed using a transmission electron microscope (TEM, JEOL JEM-2100) at an electron acceleration of 200 kV. X-ray photoelectron spectroscopic (XPS) experiments were performed with a ULVAC-PHI, Inc. Qantera XPS/AES system. UV-vis diffuse reflectance spectrometer (UV-vis DRS) were recorded in the range of 200-800 nm by a PerkinElmer LAMBDA 950 spectrophotometer. The bulk chemical compositions were measured by inductively coupled plasma-optical emission spectrometry (ICP-OES, Thermo Scientific, iCAP 6000 series). The IR spectra for the framework vibration were recorded on a FT-IR spectrometer (JEOL JIR-7000) with a resolution 4 cm^{-1} at room temperature.

Catalyst reducibility was also studied by temperature-programmed reduction (TPR) in BET-CAT Catalyst Analyzer (BEL Japan Inc.) using hydrogen (H_2). The sample were pretreated for 1h at 500 °C in synthetic air (25 ml/min) followed by cooling to 50 °C in a pure argon (Ar) stream (25 ml/min). After switching to 10 vol.% H_2 in Ar (total flow rate: 25 ml/min), temperature was increased linearly with 5 °C /min from 50 °C to 900 °C. All TPR data were normalized to the respective sample weight and expressed in arbitrary units.

Catalytic tests

The grafted catalyst (Ni-SBA-15) powders were made to pellets with size of Φ = 0.35~0.35 mm, and then pre-reduced in situ in a H_2/N_2 stream for 2 h and a heating ramp rate of 1 °C/min. The reaction was performed at atmospheric pressure in a fixed-bed quartz reactor with a 20 mm inside diameter. A 30-mm-long catalyst (2 g) between two layers of quartz wool was loaded into the reactor. A thermocouple was inserted directly into the center of the catalyst bed to measure the actual pretreatment and reaction temperatures in situ. The reactor was heated in a furnace (KTF-035N, Koyo Thermo Systems, Co., Ltd.) equipped with a temperature controller. All reactant gases were monitored with a mass flow meter (E-40) and a controller (PE-D20) (HORIBA STEC, Co., Ltd.). The flow of the product was measured with a film flow meter (VP-3, HORIBA STEC, Co., Ltd.) and analyzed with a gas chromatography-thermal conductivity detector (GC-TCD) after the methanation reaction had become stable.

3 Results and discussion

Synthesis of catalysts

The grafting of nickel (Ni) particles onto SBA-15 was first carried out using Ni ammonia (NH_3) complex ions with different NH_3/Ni mole ratios. The nitrogen adsorption/desorption isotherms of products obtained using Ni ammonia (NH_3) complex ions with different NH_3/Ni mole ratios are shown in Fig. 1 (A). In the absence of NH_4OH (NH_3/Ni mole ratio was 0), the isotherm (Fig. 1 (A) (a)) of product was exactly like that of SBA-15, a type-H1 hysteresis loop was observed in the nitrogen adsorption/desorption isotherms, the product exhibited a sharp capillary condensation step in the adsorption isotherm, suggesting that SBA-15 structure did not change. In the presence of NH_3/Ni mole ratio of 1, although the adsorption isotherm (Fig. 1 (A) (b)) of product was exactly like that of SBA-15, two hysteresis loops were found in desorption isotherm (Fig. 1 (A) (b)), similar to the post synthesis method for preparing NiO/SBA-15 with high NiO loading,[19] indicating that a blocking effect had taken place since Ni particles were grafted at the entrance of pore, and ink-bottle shaped pores were present. When NH_3/Ni mole ratios of 2~4 were employed, All isotherms (Fig. 1 (A) (c)-(e)) of products were typical for SBA-15[27] and similar to the type IV IUPAC classification,[31] a type-H1 hysteresis loop was observed in the nitrogen adsorption/desorption isotherms (Fig. 1 (A) (c)-(e)), clearly indicating that these mesoporous structures still remained. All the samples exhibited a sharp capillary condensation step in the adsorption isotherms (Fig. 1 (A) (c)-(e)), even Ni particles were grafted. However, when NH_3/Ni mole ratio was 5, the isotherm (Fig. 1 (A) (f)) of product was completely different from that of SBA-15, indicating that maybe SBA-15 structure was destroyed by NH_4OH and the serious dissolution of silica occurred. Therefore, because the dissolution of silica could be negligible, NH_3/Ni mole ratios of 2~4 were the most suitable for grafting Ni particles onto SBA-15. In addition, temperature was also varied to graft Ni particles onto

Fig. 1 Nitrogen adsorption/desorption isotherms (A) and pore size distribution (B) of SBA-15 modified with different NH_3/Ni mole ratios ((a) 0, (b) 1, (c) 2, (d) 3, (e) 4, (f) 5).

Table 1 Graft conditions and characteristics.

Sample no.	Graft conditions		Product						
			NiO						
	NH_4OH /Ni	NiO amount (wt%)	Size (nm)	Amount (wt%)	$d_{(100)}$ (nm)	S_{BET} (m^2g^{-1})	PV (cm^3g^{-1})	PD (nm)	WT (nm)
1	-	0	-	0	-	860	0.95	6.35	
2	0	10	8.0	0.80	9.85	443	0.84	6.32	5.05
3	1	10	-	4.51	-	570	0.88	6.33	
4	2	10	-	8.81	9.67	561	0.94	6.33	4.84
5	3	10	-	8.96	-	576	0.92	6.35	
6	4	10	-	8.58	9.16	562	0.89	6.32	4.27
7	5	10	-	-	-	592	0.83	4.77,6.33	
8	0	10	19.7	10	9.97	551	0.89	6.33	5.18

[a] Time = 48 h, Temperature: RT (room temperature),

[b] S_{BET}: surface area (calculated by using the Brunauer-Emmett-Teller (BET) method in the relative pressure range of p/p_0 = 0.05-0.3); PV: pore volume (obtained from the volumes of N_2 adsorbed at p/p_0 = 0.95 or in the vicinity); PD: pore diameter (analyzed by the desorption branch of the isotherms by the Barrett-Joyner-Halenda (BJH) method) and WT: wall thicknesses (calculated by $(2 \times d_{100}/\sqrt{3})$ - pore size).

SBA-15. Unfortunately, only room temperature suited for grafting Ni particles, and high temperature was likely to cause the SBA-15 structure damage. Fig. 1 (B) shows the pore size distribution (PSD) curve calculated from the desorption branch of products obtained using Ni ammonia (NH_3) complex ions with different NH_3/Ni mole ratios. In the absence of NH_4OH (NH_3/Ni mole ratio was 0), one narrow peak was observed in PSD curve, showing that a unique pore was present. In the presence of NH_3/Ni mole ratio of 1, two peaks were observed in PSD curve, which reveals a blocking effect, an ink bottle pore system not a bimodal pore system. When NH_3/Ni mole ratios were 2, one narrow peak was observed in PSD curve, showing that a unique pore was present, while when NH_3/Ni mole ratios were 3 and 4, PSD curves became broad, suggesting that a slight dissolution of silica occurred. When NH_3/Ni mole ratio was 5, three peaks were observed; indicating except a blocking effect had taken place, a new significant porosity also generated by Ni phyllosilicate phase,[15,33-35] suggesting that a serious dissolution of silica occurred, then resulted the formation of a higher proportion of Ni phyllosilicate phase. However, the biggest pore had the same size, regardless of NH_3/Ni mole ratio.

Figure 2 shows the XRD patterns of products obtained using Ni ammonia complex ions with different NH_3/Ni mole ratios. As shown in Fig 2. (A), all samples were characterized by small angle XRD as having the typical hexagonal structure of SBA-15.[27] Regardless of NH_3/Ni mole ratio, well-ordered two dimensional hexagonal structures were observed, which gave a sharp (100) plane diffraction peak and the diffraction peaks of higher Miller index planes of (110) and (200). In the wide angle XRD pattern (Fig. 2 (B) (a)) of product obtained using Ni ammonia (NH_3) complex ions with NH_3/Ni mole ratio of 0 (without NH_4OH), the peaks assigned to NiO were observed clearly, indicating that Ni particles existed as NiO, and NiO particle size calculated by XRD with the peak of 2θ = 43.3 was 8.0 nm, thus NiO/SBA-15 was obtained. However, in the wide angle XRD patterns (Fig. 2 (B) (b)-(e)) of products obtained using Ni ammonia (NH_3) complex ions with NH_3/Ni mole ratios of 1~4, no peaks assigned to NiO were confirmed, suggesting that all Ni particles were combined to silicon via oxygen (grafted onto SBA-15), in other words a chemical bond (–O–Ni–O–Si–O–) was formed between Ni and silicon via oxygen. Here, we named the products obtained with NH_3/Ni mole ratios of 1~4 by this method as Ni-grafted SBA-15 samples. However, we found that in wide angle XRD patterns (Fig. 2 (B) (b)-(e)) of Ni-grafted SBA-15 samples, the peaks originating from Ni phyllosilicate phase with low crystallinity were observed,[36] suggesting that all Ni particles were grafted onto SBA-15 to form Ni phyllosilicate phase, and the formation of Ni phyllosilicate phase was regardless of NH_3/Ni mole ratio. However the proportion of Ni phyllosilicate seemed to be related to NH_3/Ni mole ratio, namely higher NH_3/Ni mole ratio would form higher proportion of Ni phyllosilicate. Therefore, by a post synthesis method, using Ni ammonia (NH_3) complex ions with NH_3/Ni mole ratios of 1~4, Ni particles could be grafted onto SBA-15 through the formation of –O–Ni–O–Si–O–, which existed as Ni phyllosilicate phase on SBA-15 surface.[36]

Fig. 2 Small (A) and wide (B) angle XRD patterns of SBA-15 modified with different NH_3/Ni mole ratios ((a) 0, (b) 1, (c) 2, (d) 3, (e) 4).

By a template ion exchange approach,[26] in neutral media, a Ni phyllosilicate phase is formed on the part or entire external surface of MCM-41. However, in this research, in neutral media (without NH_4OH), NiO phase (Fig. 2 (A) (a)) not Ni phyllosilicate phase was formed onto SBA-15 surface, different from that previous report.[26] In this study, Ni ammonia complex ions $(Ni(NH_3)_x)^{2+}$ were formed from nickel source and NH_3 solution in basic media, which could be hydrolyzed with H_2O to form a base $Ni(OH)(NH_3)_{x-1})^+$ as pointed out in the previous report.[30] After adding SBA-15, $Ni(OH)(NH_3)_{x-1})^+$ was

Scheme 1 Ni grafted mechanism on SBA-15.

adsorbed at the ≡Si–OH surface of SBA-15 (In addition, the dissolution of silica in basic media also gave a portion of ≡Si–OH groups), and then the formation of a chemical bond –O–Ni–O–Si–O– between Ni and silicon via oxygen was completed via the reaction between $Ni(OH)(NH_3)_{x-1})^+$ and ≡Si–OH, thus resulted the isolated grafted Ni ion as Ni phyllosilicate phase as reported by Che et al.,[30] i.e. formed the grafted Ni complexes species with water (Si–O–Ni–$OH(H_2O)_x$). After calcination, another chemical bond –Si–O–Ni–O–Ni–O–Si– maybe formed through dehydration between two adjacent grafted Ni ions, namely formed the grafted polymeric and/or single Ni ion species. Therefore, the Ni grafted mechanism on SBA-15 was considered and shown in Scheme 1.

Table 1 shows grafting conditions and chemical-physical characteristics of Ni-grafted SBA-15 samples (Sample no.s: 2-7 in

Table 1) using Ni ammonia complex ions with different NH_3/Ni mole ratios. For comparison, the chemical-physical characteristic of pure SBA-15 sample (Sample no. 1 in Table 1) was also summarized in Table 1. In Table 1, the Ni amounts grafted onto SBA-15 were measured by ICP-OES. Although 10 wt% NiO was used initially, the NiO amount grafted onto SBA-15 (in product) was lower than 10 wt% (Sample no.s: 2-7 in Table 1), and depended on NH_3/Ni mole ratio. In the absence of NH_4OH, only 0.8 wt% NiO was dispersed into SBA-15 (Sample no. 2 in Table 1), suggesting that a large part of Ni source remained in mother liquid. In the presence of NH_3/Ni mole ratio of 1, only 4.5 wt% NiO was grafted onto SBA-15 (Sample no. 3 in Table 1), half of them remained in mother liquid. Only in the presence of NH_3/Ni mole ratio of 2-4, almost Ni particles were grafted onto SBA-15 (Sample no.s 4-6 in Table 1). Therefore, NiO amount modified on SBA-15 depended on NH_3/Ni mole ratio. In addition, after grafting, although there was almost no difference in pore size, the surface area and pore volume decreased. All Ni-grafted SBA-15 samples existed high special surface area, large pore volume and large pore size even Ni grafting. All the grafted materials had a typical wall thickness for SBA-15.[27]

To demonstrate the chemical nature such as the chemical and coordinate states of Ni particles in SBA-15, the Ni-grafted SBA-15 samples were studied by UV-vis and XPS. Figure 3 shows the UV-vis spectra of Ni-grafted SBA-15 samples using Ni ammonia complex ions with different NH_3/Ni mole ratios. In the presence of NH_3/Ni mole ratio of 0, a NiO absorption broad band (Fig. 3 (a)) was clearly observed in UV-vis spectrum,[37-40] indicating that all Ni species were dispersed into SBA-15 as NiO phase. When NH_3/Ni mole ratio of 1~4 was used, all the absorption bands (Fig. 3 (b)-(e)) of Ni species were shifted to lower wavelengths compared with those of bulk metal oxides, indicating the formation of a chemical bond –O–Ni–O–Si–O– between silicon and Ni via oxygen,[24] no NiO absorption band was observed.

Fig. 3 UV-vis absorbance spectra of SBA-15 modified with different NH_3/Ni mole ratios.

The Ni 2p3/2, O 1s and Si 2p XPS spectra are shown in Fig. 4. In the presence of NH_3/Ni mole ratio of 0, in Ni 2p3/2 spectrum (Fig. 4 (a), one peaks appeared at 854.5 eV could be judged to NiO,[41-50] similar to the above XRD and UV-vis results. In the presence of NH_3/Ni mole ratio of 1~4, in Ni 2p3/2 spectra of Ni-grafted SBA-15 samples, only one peak at around 856.9 eV was observed, indicating that the formation of a chemical bond –O–Ni–O–Si–O– between silicon and Ni via oxygen, no NiO particles existed, showing the formation of dispersed 2:1 nickel phyllosilicate.[36,46,50] After comparison carefully O 1s XPS spectra of products, the same result could also be observed with Ni 2p3/2 spectra of products. However, there was no obvious difference in Si 2p binding energies, regardless of NH_3/Ni mole ratio. Therefore, the information of Si 2p binding energy was not particularly helpful for the chemical identification of the local environment of Ni, only Ni 2p3/2 and O 1s binding energy was helpful.

Fig. 4 XPS spectra of SBA-15 modified with different NH_3/Ni mole ratios ((a) 0, (b) 1, (c) 2, (d) 3, (e) 4).

Fig. 5 H_2-TPR profiles of SBA-15 modified with different NH_3/Ni mole ratios ((a) 0, (b) 1, (c) 2, (d) 4).

TPR investigation is generally useful as a fingerprint of a metal species' interaction with the support material. H_2-TPR profiles are shown in Fig. 5. Without NH_4OH, H_2-TPR profile (Fig. 5 (a)) of product exhibited a broad peak centered on 379 °C, which was similar to NiO supported SBA-15,[51] indicating that NiO/SBA-15 was obtained owing to no interaction between Ni species and SBA-15. However, with NH_4OH (NH_3/Ni mole ratio of 1~4), H_2-TPR profiles (Fig. 5 (b)-(d)) of products exhibited a broad peak centered on higher temperature than NiO supported SBA-15,[51] indicating that a chemical bond –O–Ni–O–Si–O– was formed between silicon and Ni via oxygen, to reduce Ni ions, Si-O-Ni bond cleavage is required.[52] The TPR profiles are equivalent to those reported in the previous study, arising from Ni phyllosilicate.[17] Therefore, we can conclude that with NH_4OH, Ni particles were grafted onto SBA-15 from TPR studies, regardless of NH_3/Ni mole ratio.

Figure S1 shows the TG curves of Ni-modified SBA-15 samples (Fig. S1 (b)-(f)) using Ni ammonia complex ions with different NH_3/Ni mole ratios together with pure SBA-15 (Fig. S1 (a)). Compared to pure SBA-15 (Fig. S1 (a)), Ni-modified SBA-15 samples (Fig. S1(b)-(c)) gave much weight loss, but there was no almost difference (Fig. S1 (d)-(f)) in weight loss when NH_3/Ni mole ratio exceeded 2. The weight loss seemed to depend on NH_3/Ni mole ratio. In addition, the weight loss depended on Ni amount described from Table 1. Therefore, the weight loss strongly depended on Ni amount. It could be considered that the adsorbed water could increase due to Ni modified.

In addition, the weight losses at different temperature ranges were further shown in Fig. S2. As shown in Fig. S2, the change caused by Ni modified in weight loss at RT (room temperature) to 1000 °C was also confirmed, which strongly supported the above result obtained by TG. The weight loss of pure SBA-15 at RT to 120 °C, 120 to 550 °C range was less than that of SBA-15 modified with Ni. Because in SBA-15 modified with Ni, Ni particles brought a lot of adsorbed water, which could be desorbed at RT to 120 °C, thus resulted much weight loss, while the weight loss at 120 to 550 °C may be caused by condensation reaction among Ni particles. However, there was no difference in weight loss between pure SBA-15 and SBA-15 modified at 550 to 1000 °C range, indicating that thermal change cause by Ni modified had completed before 550 °C.

For further comparison, according to the previous report,[19] a conventional post synthesis (solvent (ethanol) impregnation (SI)) method was also employed to prepare highly dispersed 10 wt% NiO in SBA-15. The preparation conditions and chemical-physical characteristics of NiO dispersed SBA-15 sample are also summarized in Table 1 (Sample no. 8). In addition, the product was characterized by XRD, UV-vis, H_2-TPR, FT-IR and TEM.

Figure S3 shows the XRD patterns of Ni grafted SBA-15 sample with NH_3/Ni mole ratio of 3 and NiO dispersed SBA-15 sample using conventional post synthesis method. All samples were characterized by small angle XRD as having the typical hexagonal structure of SBA-15.[27] Regardless of preparation method, well-ordered two dimensional hexagonal structures were observed, which gave a sharp (100) plane diffraction peak and the diffraction peaks of higher Miller index planes of (110) and (200). In the wide angle XRD pattern (Fig. S3 (a)) of NiO dispersed SBA-15 using conventional method, the peaks assigned to NiO were observed clearly, indicating that Ni particles existed as NiO and NiO particle size calculated by XRD with the (111) peak of $2\theta = 37.2$ was 19.7 nm. Therefore, NiO/SBA-15 was obtained using conventional method. However, in the wide angle XRD pattern (Fig. S3 (b)) of Ni grafted SBA-15 with NH_3/Ni mole ratios of 3, no peaks assigned to NiO were confirmed, the peaks originating from Ni phyllosilicate were observed,[36] suggesting that a chemical bond was formed between

silicon and Ni via oxygen.

The UV-vis spectra of Ni-grafted SBA-15 (Ni-SBA-15) sample with NH_3/Ni mole ratio of 3 and NiO dispersed SBA-15 (NiO/SBA-15) sample using conventional post synthesis method are shown in Fig. S4. A NiO absorption broad band was clearly observed in UV-vis spectrum of NiO/SBA-15, indicating that all Ni species were dispersed into SBA-15 as NiO. However, all the absorption bands of Ni species were shifted to lower wavelengths in UV-vis spectrum of Ni-SBA-15 compared with NiO, indicating the formation of a chemical bond between silicon and Ni via oxygen, no NiO absorption band was observed.

H_2-TPR profiles of Ni-grafted SBA-15 sample with NH_3/Ni mole ratio of 3 and NiO dispersed SBA-15 sample using conventional post synthesis method are shown in Fig. S5. H_2-TPR profile (Fig. S5 (a)) of NiO dispersed SBA-15 sample exhibited a single broad peak centered on 378 °C, which was similar to NiO supported SBA-15.[51] However, H_2-TPR profile (Fig. S5 (b)) of Ni-grafted SBA-15 sample exhibited a single broad peak centered on higher temperature than NiO supported SBA-15,[51] indicating that a chemical bond was formed between silicon and Ni via oxygen, to reduce Ni ions, Si-O-Ni bond cleavage is required.[52]

FT-IR spectra of Ni-grafted SBA-15 sample obtained using NH_3/Ni mole ratio of 3 and 0 and NiO dispersed SBA-15 sample using conventional post synthesis method are shown in Fig. 6. There was almost no difference in FT-IR spectra (Fig. 6 (a)-(b)) of Ni-grafted SBA-15 sample with NH_3/Ni mole ratio of 0 and NiO dispersed SBA-15 sample, a number of bands are observed between 400 and 1400 cm^{-1}. They include the Si-O^{-1} stretching vibration of surface silanol groups at 660 cm^{-1}, a symmetric v_{Si-O} band at 796 cm^{-1}, the Si-O^- stretching vibration of surface silanol groups at 962 cm^{-1} and an asymmetric one at 1090 cm^{-1}.[53-56] The shoulder around 1190 cm^{-1} on the high-frequency side of the principal asymmetric Si-O stretch is due to an external linkage mode of the SiO_4 tetahedra.[57,58] Besides these lattice vibrations, there is a small v_{OH} mode vibrating at 3370 cm^{-1}, which is attributed to silanol SiOH unites on the SBA-15 surface with weakly acidic character.[59,60] Compared FT-IR spectrum (Fig. 6 (c)) of Ni-grafted SBA-15 sample with NH_3/Ni mole ratio of 3 with (Fig. 6 (a) and (b), no change in bands at 1090 and 1190 cm^{-1} was observed, while the decrease in bands at 796 and 660 cm^{-1} may be caused by the reaction between silianol groups and Ni particles, the increase in band at 962 cm^{-1} due to the formation of Si-O-Ni(OH), and a new band at 744 cm^{-1} appeared, indicating that a chemical bond was formed between silicon and nickel via oxygen. In addition, compared with (Fig. 6 (a) and (b), the band at 3370 cm^{-1} in Fig. 6 (c) seemed to become sharply, may be caused by Si-O-Ni-OH. In addition, FT-IR results were equivalent to the previous report.[30]

Fig. 6 FT-IR spectra of Ni-grafted SBA-15 (Ni-SBA-15) with different NH_3/Ni mole ratios of 0 (0.80 wt% NiO) (a) and 3 (8.96 wt% NiO) (c) along with 10 wt% NiO/SBA-15 (b).

TEM images of Ni-grafted SBA-15 sample with NH_3/Ni mole ratio of 3 and 0 and NiO dispersed SBA-15 sample using conventional post synthesis method are shown in Fig. 7. For Ni-grafted SBA-15 sample with NH_3/Ni mole ratio of 3, no NiO particles were observed, which typical TEM image is for SBA-15. However, in TEM images Ni-grafted SBA-15 sample with NH_3/Ni mole ratio of 0 and NiO dispersed SBA-15 sample using conventional post synthesis method, although typical TEM image is for SBA-15, NiO particles were observed clearly.

Fig. 7 TEM images of SBA-15 grafted ((a) 8.96 wt% Ni-SBA-15), supported ((b) 0.85 and (c) 10 wt% NiO/SBA-15) with NiO particles.

CO_2 Methanation

To investigate the effect of Ni particles grafted on methanation, the methanation was carried out using Ni-grafted SBA-15 catalyst (Sample no.5 in Table 1) along with NiO dispersed SBA-15 catalyst (Sample no. 8 in Table 1) obtained by conventional post synthesis method. The results are summarized and shown in Fig. 8. It is obvious Ni-grafted SBA-15 catalyst exhibited higher CO_2 conversion (TOF of 19.4 S^{-1}) than NiO dispersed SBA-15 catalyst (TOF of 16.8 S^{-1}). Therefore, when Ni particles were grafted onto SBA-15 surface, the catalytic performance was enhanced since every active center can play its catalytic role in Ni-grafted SBA-15 catalyst duo to their maximum dispersion. In addition, at methanation temperature, not every Ni particles were reduced, so Ni particles with Si-O-Ni bond maybe play an important role on CO_2 adsorption due to strong interaction, resulting that Ni-SBA-15 had higher catalytic activity than NiO/SBA-15.

Next, CO_2 methanation using Ni-grafted SBA-15 catalysts obtained with different initial NiO amounts of 4, 6, 8, 10 wt% using NH_3/Ni mole ratio of 3 were investigated. Although the results are not given in here, the CO_2 conversion and the CH_4 yield increased with increasing initial NiO amount, indicating that the Ni amount in Ni-grafted catalyst had a significantly enhanced CO_2 conversion. All Ni-grafted SBA-15 catalysts gave high CH_4 selectivity of over 90%. Using Ni-grafted SBA-15 catalyst with initial NiO amounts of 10 wt%, the maximum CO_2 conversion for methanation was obtained and which is over 80%. The maximum CH_4 yield was 73.4%, and the CH_4 selectivity was as high as 92%.

Fig. 8 TOF obtained for CO_2 methanation using Ni-grafted SBA-15 (8.96 wt% Ni-SBA-15) and NiO supported SBA-15 (10 wt% NiO/SBA-15) catalysts. Catalyst reduction conditions: temperature 550 °C (heating rate: 1 °C /min), gas flow H_2:N_2 = 120:30 ml/min, time 2 h. Reaction conditions: gas flow H_2:CO_2 = 120:30 ml/min.
TOF = (60×74.69PV/1000)/(2WtRT/100) = 9.17V/Wt,
V (ml/min): CO_2 amount converted; Wt: NiO amount (Wt%);
P: 1 atm; R: 0.082 atm•l/K•mol; T = 298 K.

Korose–Nowak criterion test: In order to establish that the measured catalytic activity is independent of the influence of transport phenomena,[61] the Korose–Nowak (KN) [62] criterion test modified by Madon–Boudart[63] has been employed. In present study, the Korose–Nowak test has been performed with Ni-grafted SBA-15 pellet catalysts with different initial NiO amounts for CO_2 methanation. Figure 9 displays the Koros–Nowak criterion plot of TOF (S^{-1}) *vs* NiO amount (wt%) for CO_2 methanation using Ni-grafted SBA-15 at 460 °C. The values of the KN numbers (slope) found to be 0.984 at 460 °C. The KN number close to unity,[61] as found in present study, denotes that reaction obeyed the KN criterion and reaction rates are not influenced by the rates of transport.

Fig. 9 The Koros–Nowak criterion plot of TOF (S^{-1}) *vs* NiO amount (wt%) for CO_2 methanation using Ni-grafted SBA-15 (Ni-SBA-15) catalysts with different NiO amount at 460 °C.
NiO amount (3.53, 5.72, 7.32, 8.56 %): Measured by ICP-OES.

The activation energies of Ni-SBA-15 catalysts with different initial NiO amounts for CO_2 methanation were calculated using Arrhenius plots at different temperatures. The relationship between activation energy of Ni-grafted SBA-15 catalyst and initial NiO amounts was shown in Fig. 10 (A). The activation energy

increased with decreasing initial NiO amounts, indicating that the initial NiO amounts in Ni-grafted SBA-15 catalyst had a significantly influence on activation energy. In addition, for comparison, the activation energy of NiO/SBA-15 catalyst was shown together, which was 96.51 KJmol^{-1} and higher than that (70.36 KJmol^{-1}) obtained using Ni-grafted SBA-15 catalyst with similar NiO amount. At methanation temperature, not every Ni particles were reduced, so Ni particles with Si-O-Ni bond maybe play an important role on CO_2 adsorption due to strong interaction, resulting Ni-SBA-15 catalysts had lower activation energy than NiO/SBA-15 catalyst. This result suggests that Ni-grafted SBA-15 catalyst had enhanced performance compared to NiO/SBA-15.

Fig. 10 Relationship between activation energy and reaction order obtained using Ni-grafted SBA-15 (Ni-SBA-15) along with NiO supported SBA-15 (10 wt% NiO/SBA-15) and NiO amount.

To obtain kinetic data for CO_2 methanation reaction, the investigation was carried out by varying the CO_2 and H_2 concentration at 460 °C using Ni-grafted SBA-15 catalysts with different initial NiO amounts. The CO_2 reaction order and the H_2 order are shown in Fig. 10 (B). There was almost no difference in CO_2 reaction order and the H_2 order caused by initial NiO amounts. The average CO_2 reaction order and the average H_2 order were 0.64, 4.05, respectively. Therefore, the rate equation could be expressed as the following: $r = kC_{CO_2}^{0.64}C_{H_2}^{4.05}$, C was concentration. Therefore, the influence of H_2 concentration was greater than CO_2 concentration on CO_2 conversion, indicating high H_2 concentration favors CO_2 conversion to methane. In addition, as shown in Fig. 10 (B), the kinetic data for CO_2 methanation reaction obtained using NiO/SBA-15 catalyst was similar to that obtained using Ni-grafted SBA-15.

Thermal stability

The thermal stability for Ni-grafted SBA-15 sample using NH_3/Ni mole ratio of 3 was investigated by calcination at different temperatures, and the results are shown in Fig. 11 (A). Even with calcination at 700 ℃ (Fig. 11 (A) (a), almost no NiO particles were observed in XRD pattern of Ni-grafted SBA-15 sample. However, after alcination at 750 ℃, NiO particles were observed clearly (Fig. 11 (A) (b), indicating that the chemical bond –O–Ni–O–Si–O– was broken and NiO particles were formed. Therefore, Ni-grafted SBA-15 sample had high thermal stability.

Fig. 11 XRD patterns of (A) Ni-grafted SBA-15 (8.96 wt% Ni-SBA-15) calcined at different temperature ((a) 700 °C, (b) 750 °C) and (B) NiO supported SBA-15 (10 wt% NiO/SBA-15, (a)) and Ni-grafted SBA-15 (8.96 wt% Ni-SBA-15, (b)) after methanation.

The thermal stability for Ni-grafted SBA-15 sample using NH_3/Ni mole ratio of 3 was also studied by N_2 adsorption after calcinations at different temperatures and after methanation, and the results are shown in Fig 12 (A). There was almost no difference in N_2 adsorption before and after methanation, indicating Ni-grafted SBA-15 catalyst possessed high thermal stability for methanation. The obvious decrease in N_2 adsorption was observed after calcination for Ni-grafted SBA-15 sample, but the adsorbed amount did not decrease with increasing calcination temperature, and that increased after calcination at 750 °C compared with calcination at 700 °C, suggesting that the cleavage of chemical bond between silicon and nickel increased the surface area.

For comparison, the study on thermal stability of NiO dispersed SBA-15 sample obtained with a conventional post synthesis method was also carried out using XRD after methanation, and Figure 11(B) shows the result along with that of Ni-grafted SBA-15 sample. Whether NiO dispersed SBA-15 (Fig. 11 (B) (a)) or Ni-grafted SBA-15 (Fig. 11 (B) (b)), Ni particles were observed clearly in all XRD patterns. However, for NiO dispersed SBA-15 (Fig. 11 (B)(a)), the peak intensities of Ni particles were higher than that for Ni-grafted SBA-15 (Fig. 11 (B) (b)), indicating the amounts of Ni particles reduced for NiO dispersed SBA-15 (Fig. 11 (B) (a)) were more than that for Ni-grafted SBA-15 (Fig. 11 (B) (b)). In our catalytic section, Ni-grafted SBA-15 catalyst had higher conversion than NiO dispersed SBA-15, therefore, even Ni-grafted SBA-15 catalyst with less Ni particles can achieved higher performance than NiO dispersed SBA-15 with more Ni particles . In addition, the N_2 adsorption of NiO dispersed SBA-15 catalyst before and after methanation was carried out and displays in Fig. 12 (B). There was almost no difference in N_2 adsorption before and after methanation, indicating NiO dispersed SBA-15 catalyst possessed high thermal stability for methanation, like to Ni-grafted SBA-15 catalyst.

Fig. 12 Nitrogen adsorption/desorption isotherms of (A) Ni-grafted SBA-15 (8.96 wt% Ni-SBA-15) calcined at different temperature, before and after methanation; and (B) NiO supported SBA-15 (10 wt% NiO/SBA-15) before and after methanation.

4 Conclusions

Ni particles were grafted onto SBA-15 by a post synthesis method using Ni ammonia (NH_3) complex ions $(Ni(NH_3)_x)^{2+}$ with NH_3/Ni mole ratio of 2~4, which was named Ni-grafted SBA-15 sample. XPS, UV-vis and H_2-TPR analyses demonstrated that a chemical bond was formed between Ni and silicon via oxygen in Ni-grafted SBA-15 samples. CO_2 methanation was carried out using Ni-grafted SBA-15 catalyst, resulting in high CO_2 conversion and methane selectivity. Kinetic study for CO_2 methanation reaction shown the activation energy depended on initial Ni amount, the rate equation for CO_2 methanation could be expressed as: $r = kC_{CO_2}^{0.64}C_{H_2}^{4.05}$, C was concentration. Compared to NiO dispersed SBA-15 catalyst obtained by conventional post synthesis method, Ni-grafted SBA-15 catalyst exhibited excellent catalytic efficiency. Ni-grafted SBA-15 catalyst had high thermal stability for CO_2 methanation.

Notes and References

1 C. Liang, Z. Li and S. Dai, *Angew. Chem., Int. Ed.*, 2008, **47**, 3696.
2 A. Corma, *Chem. Rev.*, 1997, **97**, 2373.
3 V. Parvulescu and B.-L. Su, *Catal. Today*, 2001, **69**, 315.
4 Y. Yang, S. Lim, G. Du, Y. Chen, D. Ciuparu and G. L. Haller, *J. Phys. Chem. B*, 2005, **109**, 13237.
5 Y. Park, T. Kang, J. Lee, P. Kim, H. Kim and J. Yi, *Catal. Today*, 2004, **97**, 195.
6 U. Junges, S. Disser, G. Schmid and F. Schüth, in: L. Bonneviot, F. Béland, C. Danumah, S. Giasson and S. Kaliaguine (Eds.), *Mesoporous Molecular Sieves* 1998, *Studies in Surface Science and Catalysis*, vol. **117**, Elsevier, Amsterdam, 1998, p. 391.
7 B. -W. Lu and K. Kawamoto, *RSC Adv.*, 2012, **2**, 6800.
8 T. Linssen, K. Cassiers, P. Cool and E. F. Vansant, *Adv. Colloid Interface Sci.*, 2003, **103**, 121.
9 M. Kruk, M. Jaroniec, R. Ryoo and J. -M. Kim, *Micropor. Mater.*,

1997, **12**, 93.
10 J. F. Bengoa, M. V. Cagnoli, N. G. Gallegos, A. M. Alvarez, L. V. Mogni, M. S. Moreno and S. G. Marchetti, *Micropor. Mesopor. Mater.*, 2005, **84**, 153.
11 A. Lewandowska, S. Monteverdi, M. Bettahar and M. Ziolek, *J. Mol. Catal. A Chem.*, 2002, **188**, 85.
12 R. Wojcieszak, S. Monteverdi, M. Mercy, I. Nowak, M. Ziolek and M. M. Bettahar, *Appl. Catal. A: Gen.*, 2002, **268**, 241.
13 K. Fang, W. Wei, J. Ren and Y. Sun, *Catal. Lett.*, 2004, **93 (3–4)**, 235.
14 R. B. Biniwale, N. Kariya and M. Ichikawa, *Catal. Lett.*, 2005, **105 (1–2)**, 83.
15 P. Burattin, M. Che and C. Louis, *J. Phys. Chem. B*, 1997, **101 (36)**, 7060.
16 P. Burattin, M. Che and C. Louis, *J. Phys. Chem. B*, 1999, **103 (30)**, 6171.
17 P. Burattin, M. Che and C. Louis, *J. Phys. Chem. B*, 1998, **102 (15)**, 2722.
18 M. Hartman, A. Poeppl and L. Kevan, *J. Phys. Chem.*, 1996, **100**, 9906.
19 B. -W. Lu and K. Kawamoto, *Fuel*, 2013, **103**, 699.
20 C. K. Vance and C. H. Bartholomew, *Appl. Catal. A: General*, 1983, **7**, 169.
21 C. T. Kresge, M. E. Leonowicz, W. J. J. C. Vartuli and J. S. Beck, *Nature*, 1992, **359**, 710.
22 Á. Szegedi, M. Popova, V. Mavrodinova, M. Urbán, I. Kiricsi and C. Minchev, *Micropor. Mesopor. Mater.*, 2007, **84**, 149.
23 G. Du, S. Lim, Y. Yang, C. Wang, L. Pfefferle and G. L. Haller, *J. Catal.*, 2007, **249**, 370.
24 D. Liu, R. Lau, A. Borgna and Y. Yang, *Appl. Catal.A: Gen.*, 2009, **358**, 110.
25 B.-W. Lu and K. Kawamoto. Catal. Sci. Technol., 2014, **4**, 4313.
26 T. Lehmann, T. Wolff, C. Hamel, P. Veit, B. Garke and A. Seidel-Morgenstern, *Micropor. Mesopor. Mater.*, 2012, **151**, 113.
27 D. Zhao, J. Feng, Q. Huo, N. Melosh, G. H. Fredrickson, B. F. Chmelka and G. D. Stuchy, *Science*, 1998, **279**, 548.
28 B.-W. Lu and K. Kawamoto, *J. Environ. Chem. Eng.*, 2013, **1**, 300.
29 C. K. Vance and C. H. Bartholomew, *Appl. Catal. A: General*, 1983**, 7**, 169.
30 O. Clause, M. Kermarec, L. Bonneviot, F. Villain and M. Che, *J. Am. Chem. Soc.* 1992, **114**, 4709.
31 B. -W. Lu, Y. Inagi and A. Endo, *J. Nanosci. Nanotechnol.*, 2011, **11**, 2361.
32 S. J. Gregg and K. S. W. Sing, *Adsorption Surface Area and Porosity*, Academic Press, New York, 1982.
33 A. Gil, A. Diaz, L. M. Gandia and M. Montes, *Appl. Catal. A*, 1994, **109**, 167.
34 L. A. M. Hermans and J. W. Geus, in: B. Delmon, P. Grange, P. A. Jacobs and G. Poncelet (Eds.), *Preparation of Catalysts II*, vol. **3**, Elsevier, Amsterdam, 1979, pp. 113.
35 D. G. Blackmond and E. I. Ko, *Appl. Catal.*, 1984, **13**, 49.
36 S. M. V. Sivaiah, S. Petit, M. F Beaufort, D. Eyidi, J. Barrault, C. Batiot-Dupeyrat and S. Valange, *Micropor. Mesopor. Mater.*, 2011, **140**, 69.
37 M. Marciuš, M. Ristic, M. Ivanda and S. Music, *J. Mol. Struct.*, 2013, **1044**, 231.
38 B. Scheffer, J. J. Heijeinga and J. A. Moulijn, *J. Phys. Chem.*, 1987, **91**, 4752.
39 C. Lepetit and M. Che, *J. Phys. Chem.*, 1996, **100**, 3137.
40 D. P. Liu, X. Y. Uuek, W. N. E. Cheo, R. Lau, A. Borgna and Y. H. Yang, *J. Catal.*, 2009, **266**, 380.
41 T. L. Barr, *J. Phys. Chem.*, 1978, **82**, 1801.
42 K. S. Kim and N. Winograd, *Surf. Sci.*, 1974, **43**, 625.
43 R. B. Shalvoy, P. J. Reucroft and B. H. Davis, J. Catal., 1979, **56**, 336.
44 M. F. Wilson, P. R. Mainwaring, J. R. Brown and J. F. Kriz, *Appl. Catal.*, 1998, **41**, 177.
45 P. Dufresene, E. Payen, J. Grimblot and J. P. Bonnelle, *J. Phys. Chem.*, 1981, **85**, 2344.
46 P. Lorenz, J. Finster, G. Wendt, J. V. Salyn, E. K. Zumadilov and V. I. Nefedov, *J. Electron. Spectrosc. Relat. Phenom.*, 1979, **16**, 267.
47 A. S. Al-Ubaid, *Ind. Eng. Chem. Res.*, 1988, **27**, 790.
48 M. L. Occelli, D. Psaras, S. L. Suib and J. M. Stencel, *Appl. Catal.*, 1986, **28**, 143.
49 J. C. Vedrine, G. Hollinger and T. M. Duc, *J. Phys. Chem.*, 1978, **82**, 1515.
50 G. Wendt, D. hentschel, J. Finster, R. Schollner, S. Hanafi and R. S. Mikhail, *J. Chem. Soc. Faraday Trans.*, 1983, **179**, 2013.
51 M. -Y. Cheng, C. -J. Pana and B. -J. Hwang, *J. Mater. Chem.*, 2009, **19**, 5193.
52 O. Clause, L. Bonneviot and M. Che, *J catal.*, 1992, **138**, 195.
53 M. Broyer, S. Valange, J. P. Bellat, O. Bertrand, G. Weber and Z. Gabelica, *Langmuir*, 2002, **18**, 5083.
54 M. A. Camblor, A. Corma and J. Perez-Pariente, *J. Chem. Soc., Chem. Commun.*, 1993, 557.
55 M. Decottignies, J. Phalippou and J. Zarzycki, *J. Mater. Sci.*, 1978, **13**, 2605.
56 M. Ocana, V. Fornes and C. J. Serna, *J. Non-Cryst. Solids*, 1989, **107**, 187.
57 S. M. Holmes, V. L. Zholobenko, A. Thursfield, R. J. Plaisted and C. S. Cundy, *J. Dwyer, J. Chem. Soc., Faraday Trans.*, 1998, **94**, 2025.
58 E. M. Flanigen, H. Khatami and H. A. Szymanski, in: E. M. Flanigen and L. B. Sand (Eds.), *Molecular Sieve Zeolites-I*, American Chemical Society, Washington, DC, 1974, pp. 201.
59 J. Chen, Q. Li, R. Xu and F. Xiao, *Angew. Chem., Int. Ed.*, 1995, **34**, 2694.
60 A. Jentys, N. H. Pham and H. Vinek, *J. Chem. Soc., Faraday Trans.*, 1996, **92**, 3287.
61 P. Arnoldy and J. A. Moulijn, *J. Catal.*, 1985, **93**, 38.
62 Lj. Kundakovic and M. Flytzani-Stephanopoulos, *Appl. Catal. A: General*, 1998, **171**, 13.
63 E. Sols, *Coll. Chem. Commun. Czech.*, 1962, **27**, 2621.

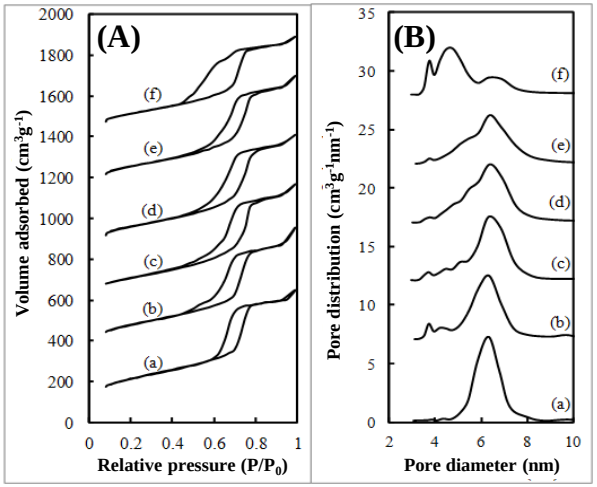

Fig. 1

LU et al.

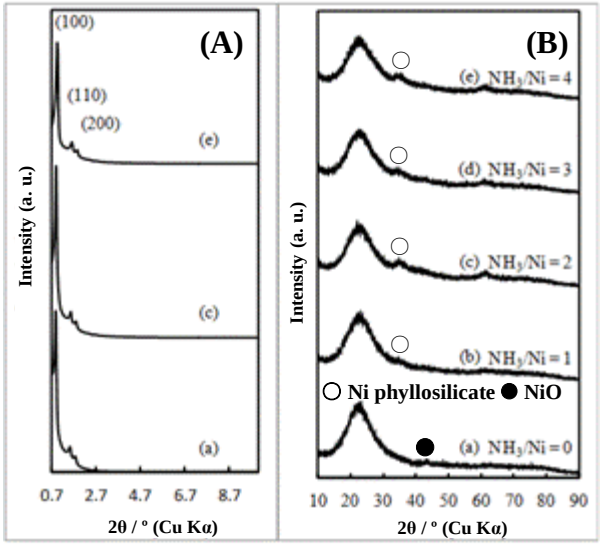

Fig. 2

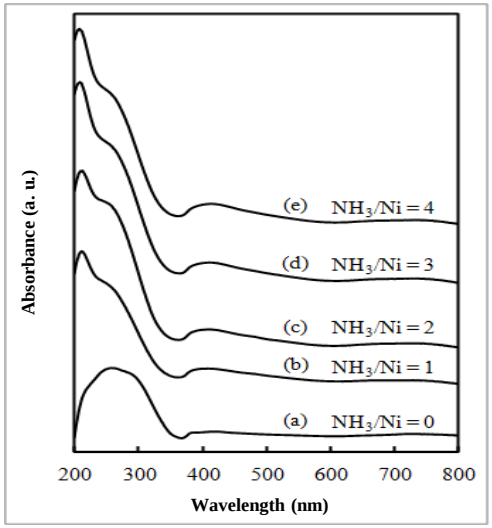

Fig. 3 **LU et al.**

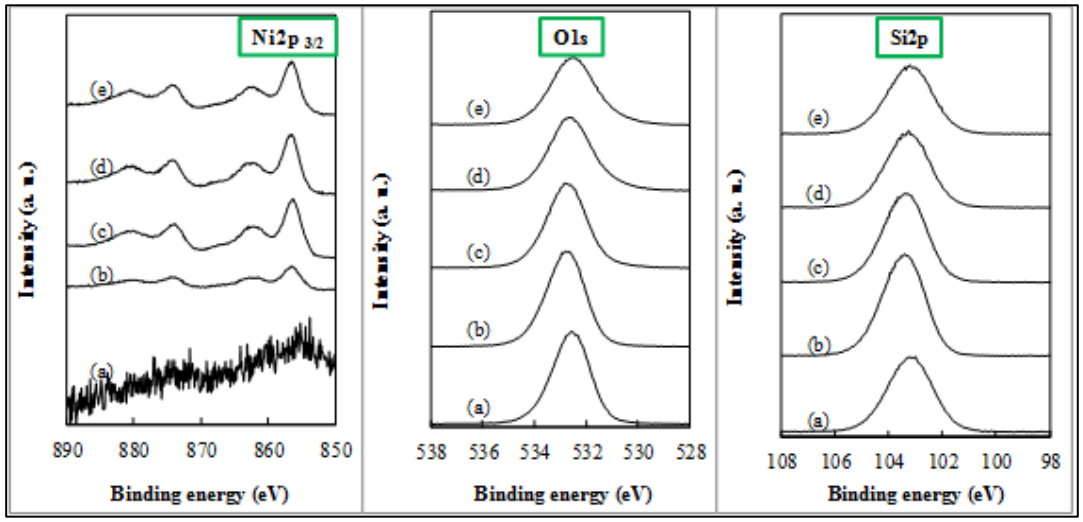

Fig. 4

LU et al.

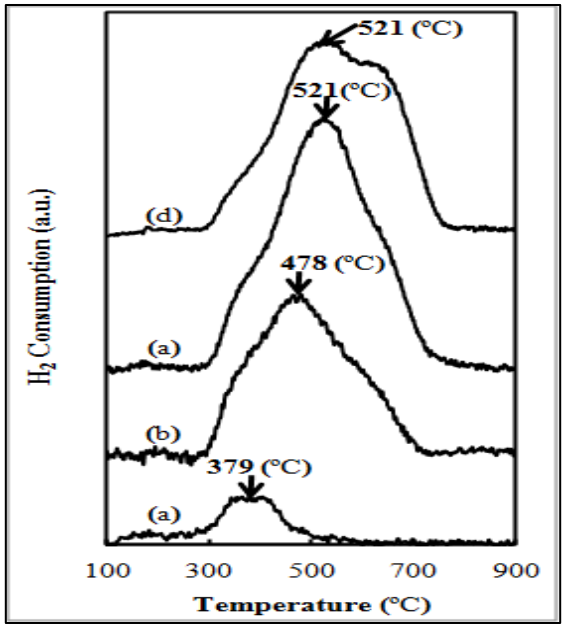

Fig. 5

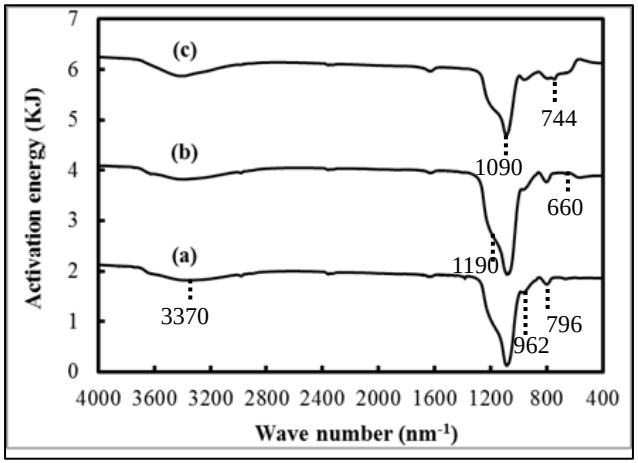

Fig. 6

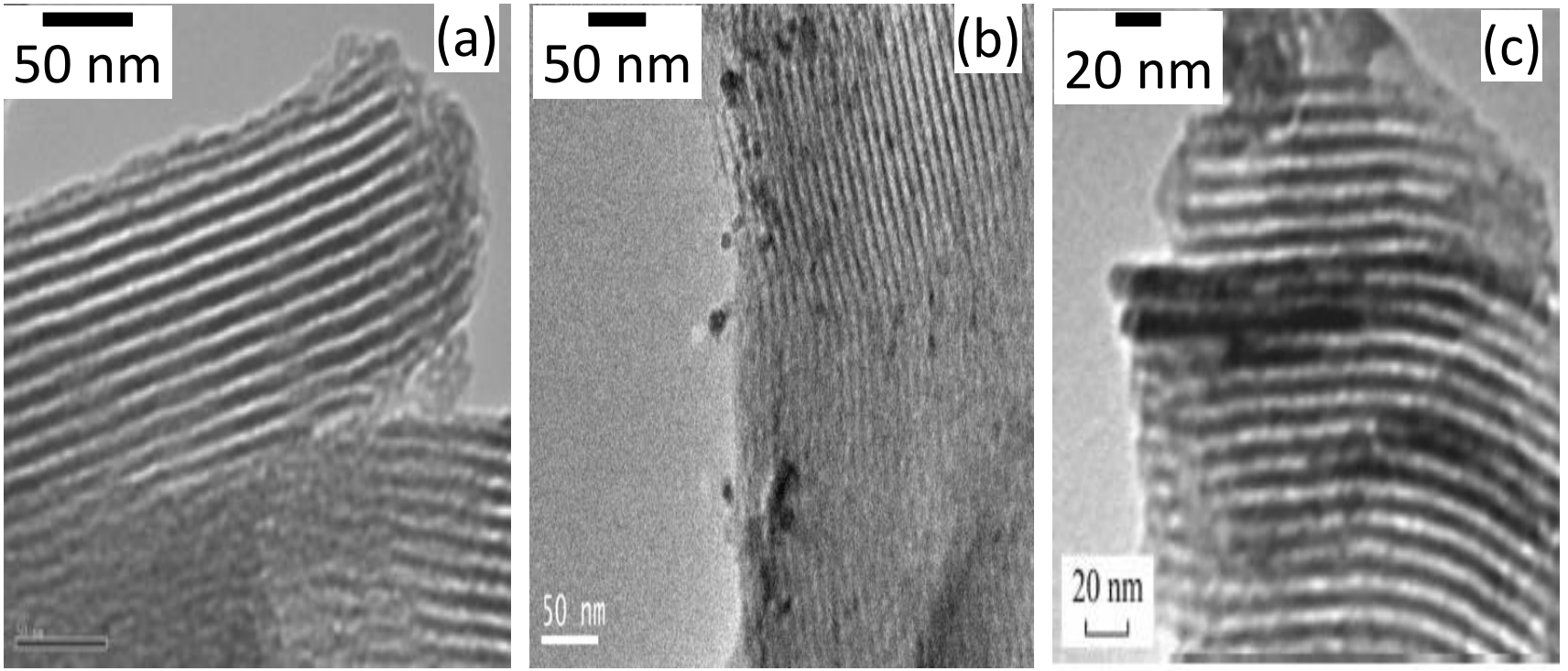

Fig. 7 LU et al.

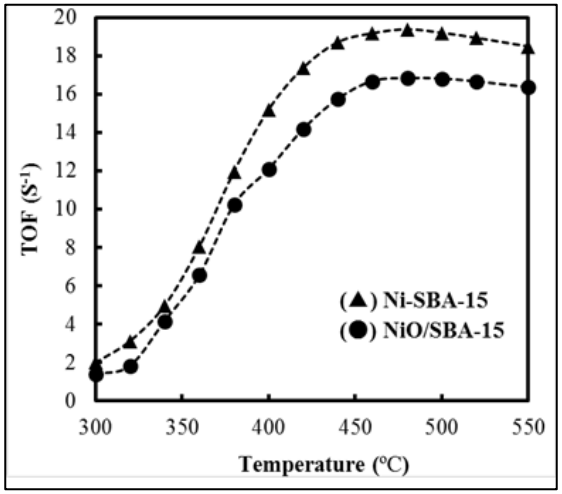

Fig. 8

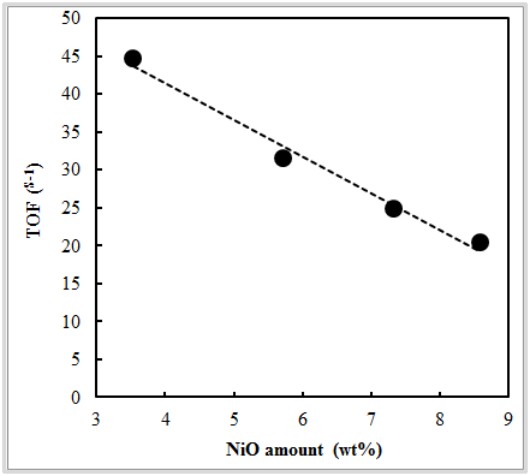

Fig. 9 LU et al.

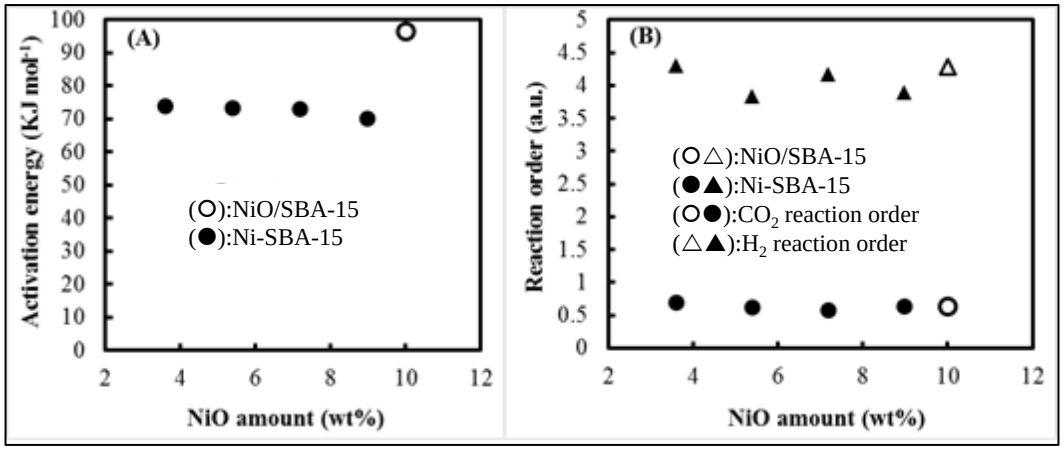

Fig. 10

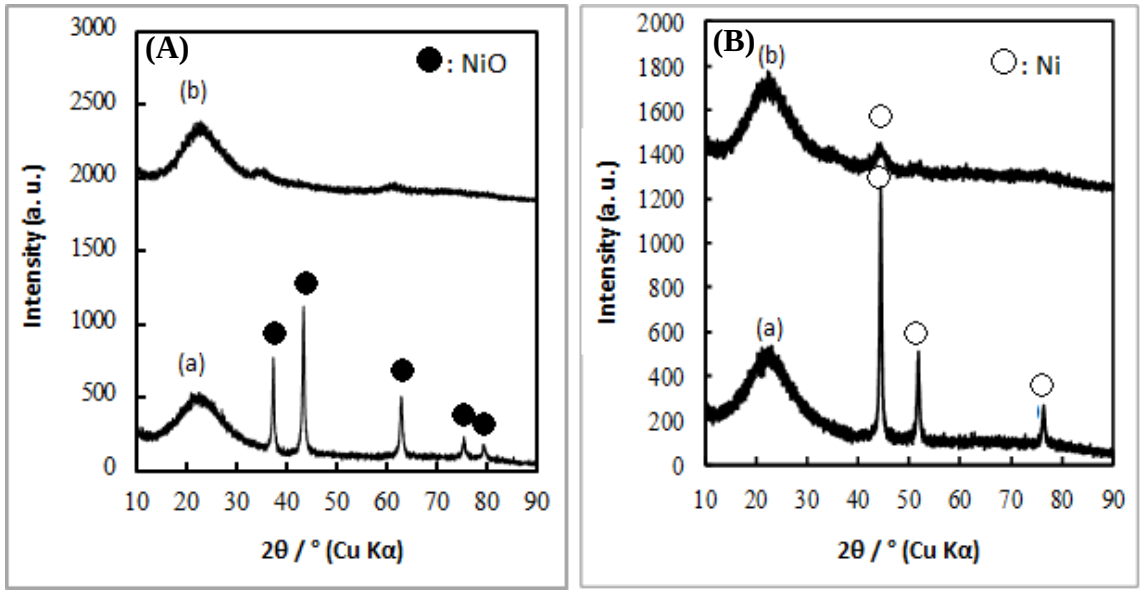

Fig. 11 LU et al.

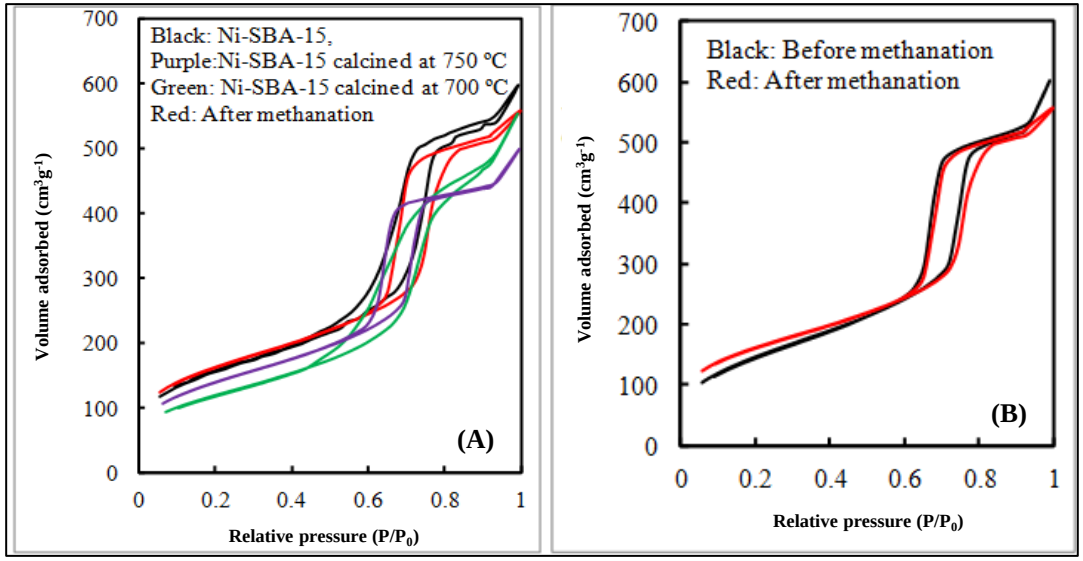

Fig. 12 **LU et al.**

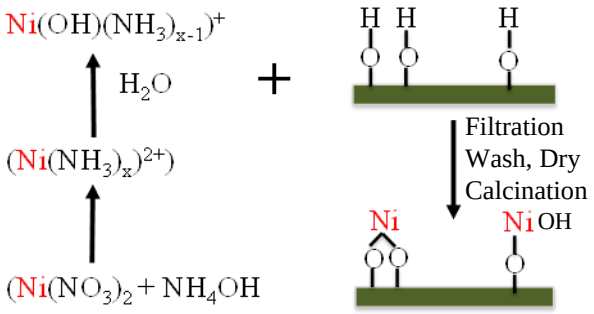

Scheme 1

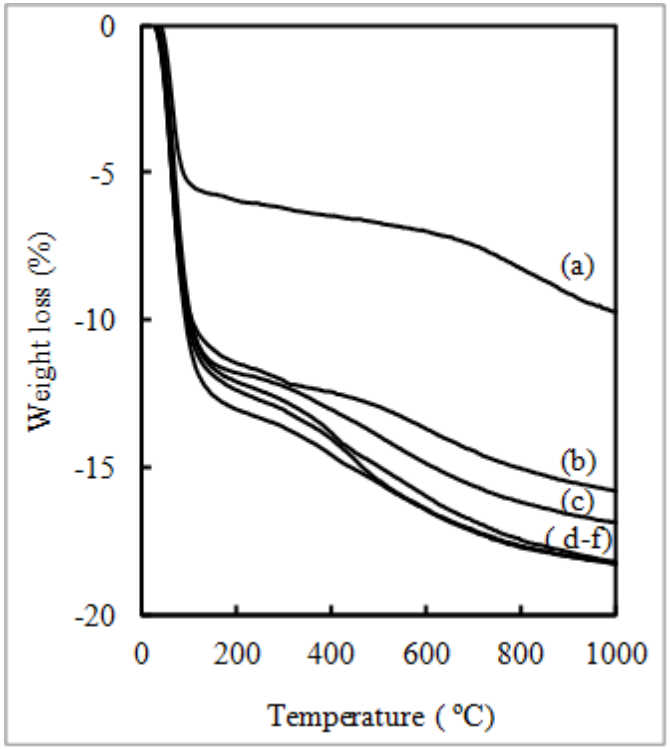

Fig. S1

LU et al.

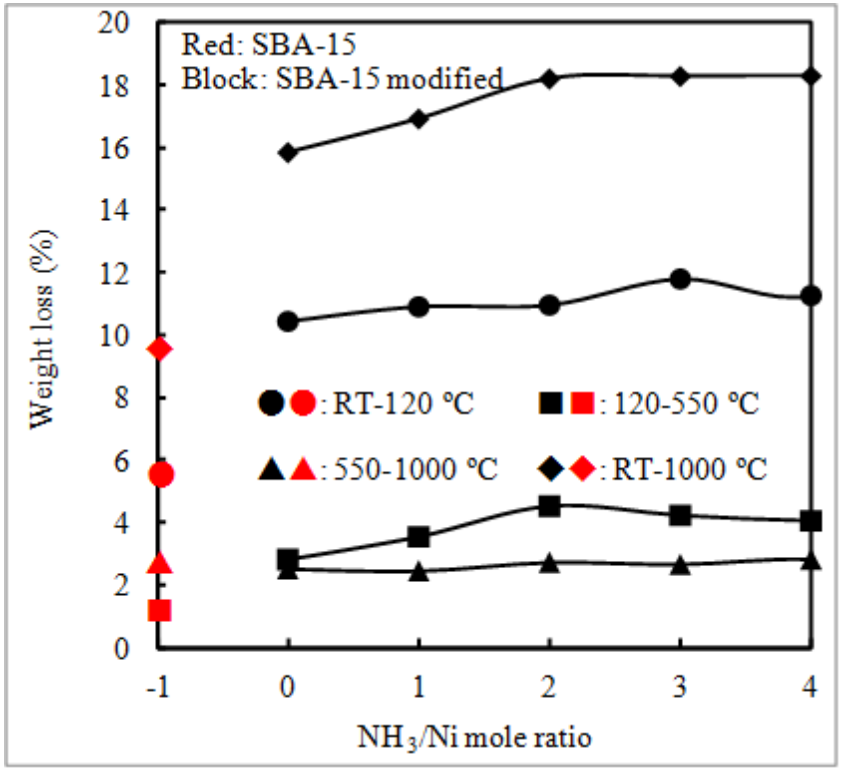

Fig. S2

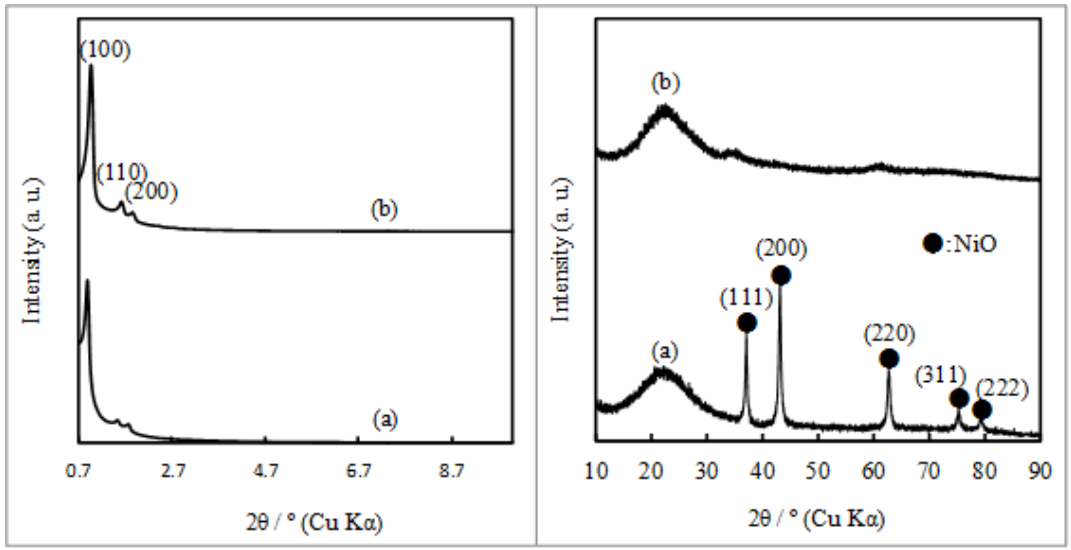

Fig. S3 **LU et al.**

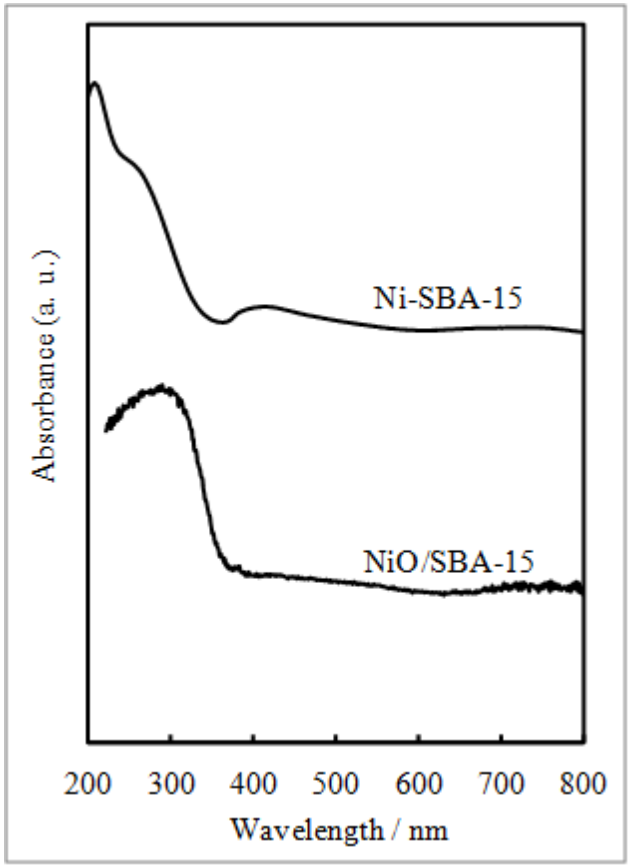

Fig. S4

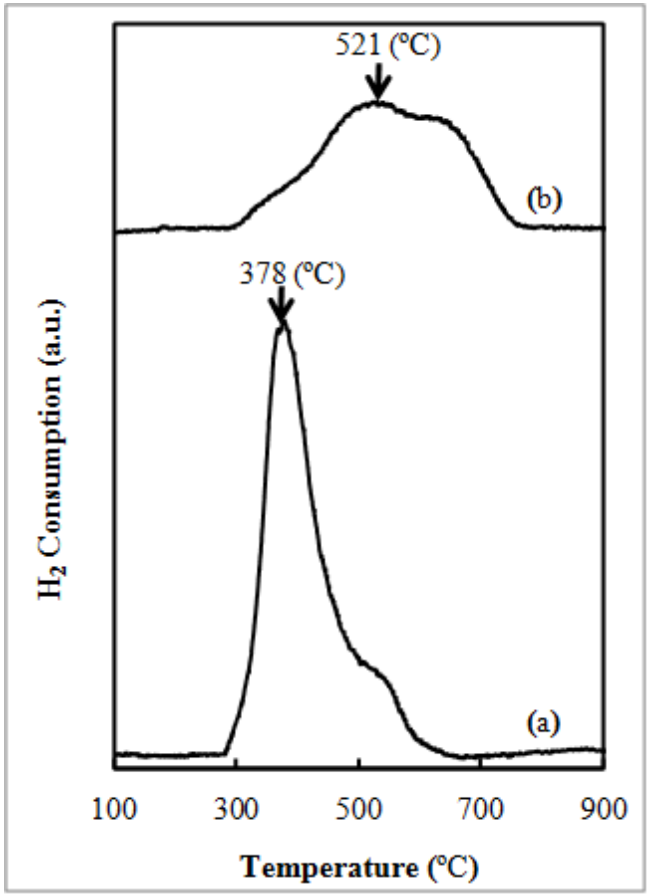

Fig. S5 LU et al.